A Thesis

on

PREPARATION OF TiO_2 NANOPARTICLES VIA GLYCOLATE ROUTE

and

EFFECT OF ADDITION OF ALCOHOL ON PARTICLE MORPHOLOGY

Submitted in the partial fulfillment of requirement for the award of the

Degree of

Master of Science (PHYSICS)

Submitted by: **CHARU KAMAL**

Roll No.: 300804004

Under the Guidance of

Ms. Loveleen K. Brar

School of Physics and Materials Science (SPMS)

THAPAR UNIVERSITY

PATIALA (PUNJAB)-147 004

JULY 2010

Dedicated

To

My Loving Parents

DECLARATION

I hereby declare that thesis entitled "**Preparation of TiO_2 nanoparticles via glycolate route and effect of addition of alcohol on the particle morphology**" is the original work carried out by me under the supervision of **Ms. Loveleen K. Brar.** The matter embodied in this thesis has not been submitted anywhere else for the award of any degree.

Ms. Charu Kamal
300804004
M. Sc. (Physics)

CERTIFICATE

This is to certify that thesis entitled "**Preparation of TiO_2 nanoparticles via glycolate route and effect of addition of alcohol on the particle morphology**" submitted by Ms. Charu Kamal (Roll no.-300804004) of M.Sc. (Physics), Thapar University, Patiala was carried out by her under the supervision of Ms. Loveleen K. Brar. She has not submitted this material for credit towards any other degree at this or any other university.

Supervisor

Loveleen Kaur Brar 15/7/10

Ms. Loveleen K. Brar
Astt. Professor
School of Physics and Material Science
Thapar University, Patiala

Countersigned by

Dr. O. P. Pandey
Professor and Head
School of Physics and Material Science
Thapar University, Patiala

Dr. R. K Sharma 22/7
Dean of Academic Affairs
Thapar University, Patiala

ACKNOWLEDGEMENT

This piece of work would not have been accomplished without the blessings and power given to me by Almighty and people behind my life for inspiring, guiding and accompanying me.

Foremost, I would like to express my sincere gratitude to my esteemed and worthy supervisor **Ms. Loveleen K. Brar**, Astt. Professor, School of Physics and Material Science, for her consistent support, patience, motivation, enthusiasm and giving immense knowledge in my thesis work. Her guidance helped in all time of research and writing this thesis.

I would also express my deep sense of gratitude towards **Dr. K. K. Raina, Dr. N. K. Verma and Dr. O. P. Pandey** for allowing use of their lab facilities.

Besides them I would like to thank **Mr. Ravi Shukla**, research scholar, for his immense help in carrying out experimental work and discussion of data at different stages of my thesis work.
Also I would thank **Mr. Purushottam Singh** for providing X-Ray Diffraction data.

Last but not the least, I would like to extend my heartful gratitude to my parents. My project would not have seen daylight without their immense cooperation and moral support of my parents who kept my spirits high during the endeavour.

Charu Kamal

ABSTRACT

Various methods have been employed to improve the size and properties of the TiO_2 nanoparticles so as to enhance the performance of TiO_2 based materials. In the present work TiO_2 nanoparticles have been synthesized via the glycolate route. We have studied the effects of tertiary-Butanol as a capping agent to limit the size of the TiO_2 nanoparticles. Glycolate route involves the formation and subsequent calcination of Titanium-glycolate (TiG) coordination complexes. This method offers advantages in terms of phase purity and formation of mono-dispersed particles. Titanium(IV) butoxide, $Ti[O(CH_2)_3CH_3]_4$ was added to a mixture of Ethylene Glycol and tert-Butanol and heated at 160°C for 2 hrs with constant stirring using a magnetic stirrer. The alkoxide was transformed into the glycolate complex. The crystallites could be readily collected as precipitates after the reaction solution had been cooled down to room temperature. The formation of TiG is confirmed by FT-IR. The molar ratios of Titanium(IV) butoxide : Ethylene Glycol : tert-Butanol were varied for different samples. In each case the TiG precursor formed is further characterized by DTA and TGA. By calcining at 500 °C and 850 °C temperatures, each TiG precursor could be transformed into anatase and rutile phases of TiO_2, respectively. The crystal structure, lattice parameters and the average crystallite size of the samples have been calculated using X-ray diffraction pattern and TEM, respectively. The particle size has decreased as the ratio of tert-Butanol : EG increases. This is a confirmation of the capping properties of the tert-butanol.

LIST OF CONTENTS

LIST OF FIGURES

LIST OF TABLES

LIST OF ABBREVATIONS

NAME OF CHEMICALS	CHEMICAL FORMULA	ABBREVIATIONS
Titanium dioxide	TiO_2	Titania
Titanium glycolate	$Ti(OCH_2CH_2O)_2$	TiG
Ethylene glycolate	$HOCH_2CH_2OH$	EG
Titanium(IV) butoxide	$Ti[O(CH_2)_3CH_3]_4$	Ti-but
Tertiary butanol	$C_4H_{10}O$	Tert-butanol
Barium Titanium glycolate	$BaTi(C_2H_4O_2)_3.4C_2H_6O_2.H_2O$	BTG
Barium Titanate	$BaTiO_3$	Ba-titanate
Thermogravimetric Analysis	___	TGA
Differential Thermal Analysis	___	DTA
Fourier Transform Infrared microscopy	___	FTIR
X-Ray Diffraction	___	XRD
Transmission Electron Microscopy	___	TEM

CHAPTER 1

INTRODUCTION

1.1 NANOPARTICLES

Nanoparticles are of a great scientific interest since they are effectively a bridge between bulk materials and atomic or molecular structures. They have properties that are between those of bulk and those of discrete molecules. A bulk material generally has constant physical properties regardless of its size, but at the nano-scale, this is often not the case. Size-dependent properties (e.g. quantum confinement in semiconductor particles, surface plasmon resonance in some metal particles, etc.) are often observed [1]. The properties of materials change as their size approaches the nanoscale and the percentage of atoms at the surface of a material becomes significant. Nanoparticles have a very high surface area to volume ratio [2, 3].

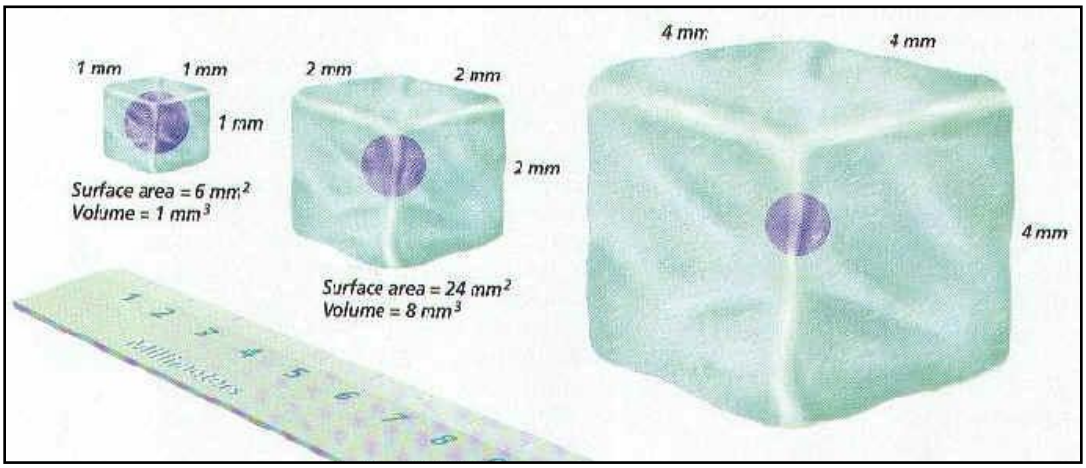

Fig. 1.1 Example to illustrate increase in Surface to volume ratio [4]

Almost all materials system including metals, insulators and semiconductors show size dependent electronic or optical properties in the quantum size regime. Among these, the modification in the energy band gap of semiconductors is the most attractive one because of the fundamental as well as technological importance [5]. The band gap can be controlled with the change in size of the nanomaterial, so the different colored emission can be observed from the same material. Thus, quantum dots of same material can be used for fabrication of LEDs having emission over the whole visible spectrum [6, 7].

1.2 Titanium Dioxide (TiO_2)

Titanium dioxide, also known as Titanium(IV) oxide or titania, is the naturally occurring oxide of titanium, chemical formula TiO_2 [10]. TiO_2 has been reported as one of the most suitable semiconducting materials in a wide range of technological applications, such as photo-catalyst, because of its photo-catalytic activity through the irradiation of light at the surface. It has been embraced as an inexpensive, with high surface-to-volume ratio, non-toxic material. The properties of TiO_2 are influenced by the crystal structure, surface area, band gap, size distribution, crystallinity, porosity and surface hydroxyl group density [8].

1.2.1 Occurrence

Pure titanium dioxide does not occur in nature but is derived from ilmenite or leuxocene ores. It is also readily mined in one of the purest forms as rutile beach sand. Titanium dioxide occurs in nature as well-known mineral forms rutile, anatase and brookite, and additionally as two high pressure forms, a monoclinic baddeleyite-like form and an orthorhombic α-PbO_2-like form, both found recently at the Ries crater in Bavaria. The most common form is rutile, which is also the most stable form. Anatase and brookite both convert to rutile upon heating [14].

PHASE	CRYSTAL SYSTEM
Rutile	Tetragonal
Anatase	Tetragonal
Brookite	Orthorhombic

Table 1.1 Crystal systems of different phases of TiO_2

1.2.2 Structure of TiO_2

Rutile and Anatase structures can be defined in terms of chains of TiO_6 octahedral, where each Ti^{4+} ion is surrounded by an octahedron of six O^{2-} ions. The two crystal structures differ in the distortion of each octahedron and by the assembly pattern of the octahedral chains.

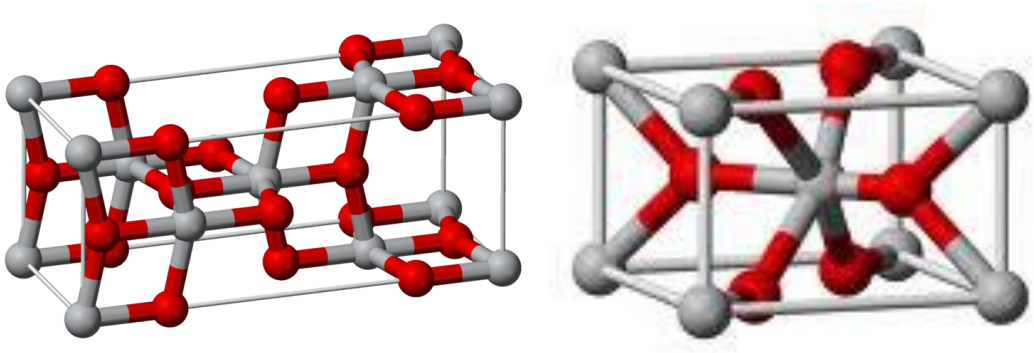

(a) (b)

Fig.1.2 Crystal Structure of a) Anatase phase and b) Rutile phase [9, 10]

RUTILE : Each octahedron shares corner with **eight** neighbors and shares edges with two other neighbors, forming a linear chain.

ANATASE: Each octahedron shares corners with **four** neighbors and shares edges with four other neighbors, forming a zig-zag chain with a screw axis [11].

Rutile is the more common and the more well known mineral of the three, while anatase is the rarest. Metal-metal interaction is large in case of anatase (5.35Å) and smaller in case of rutile (2.96Å). These differences in lattice structures cause different mass densities and electronic band structures between the two forms of TiO_2.

Chemical Formula	TiO_2
Molecular Weight	79.9
Crystal Class	Tetragonal
Density, g/cm^3 at 300 K	4.25
Transmission Range, µm	0.43 - 6.2
Reflection Loss for two surfaces at 2µm,% for the ordinary ray for the extraordinary ray	 30 34.8
Zero Dispersion Wavelength, µm	2.8

Dielectric Constant for 10^4 - 10^7 Hz	200-160
Melting Temperature, K	2090
Thermal Conductivity, W/(m K) at 273 K parallel perpendicular	 13.9 9.0
Thermal Expansion, 1/K at 313 K parallel perpendicular	 9.2×10^{-6} 7.1×10^{-6}
Specific Heat, cal/(g K) at 298 K	0.17
Bangap, eV	3.3

Table 1.2 General Properties of TiO_2 [12]

1.2.3 Applications of TiO_2

1. TiO_2 is also an effective opacifier in powder form, where it is employed as a pigment to provide whiteness and opacity to products such as paints, coatings, plastics, papers, inks, foods, medicines (i.e. pills and tablets) as well as most toothpastes.
2. In cosmetic and skin care products, titanium dioxide is used both as a pigment, sunscreen and a thickener because of its high refractive index (n = 2.7), its strong UV light absorbing capabilities and its resistance to discolouration under ultraviolet light [11].
3. Titanium dioxide, particularly in the anatase form, is a photo-catalyst under ultraviolet (UV) light. TiO_2 is most efficient and environmentally benign photo-catalyst. It is a semiconductor which turns to a high energy state by receiving light energy, and releases electrons from its illuminated surface. If the energy received at this stage is high enough, electrons that are initially located in the valence band all jump up to the conduction band. The electron hole pair is generated, which generate free radicals able to undergo secondary reaction. This forms the principle of photo-catalytic activity of photo generated

catalysis. The hole produced has strong oxidizing power and the electrons have strong reducing power. Due to this, it has wide applications in food testing labs, medical fields etc [11].

The photo-catalyst activity of a semiconductor is largely controlled by:

a) The light absorption properties like light absorption spectrum and coefficient.
b) Reduction and oxidation rates on the surface by electron and hole.
c) Electron hole recombination rate.

A large surface area with a constant surface density of absorbents leads to faster surface photo-catalytic reaction rate. On the other hand, the surface is defective site, therefore, large the surface area, the faster the recombination. The higher the crystallinity, the fewer the bulk defects, and the higher the photo-catalytic activity is.

4. Used for Anti-fogging glasses, self cleaning glass, anti-bacterial, anti-viral, fungicidal, anti-soiling, self cleaning, deodorizing, air purification, water treatment, water purification.
5. Used in electronic components like capacitors.

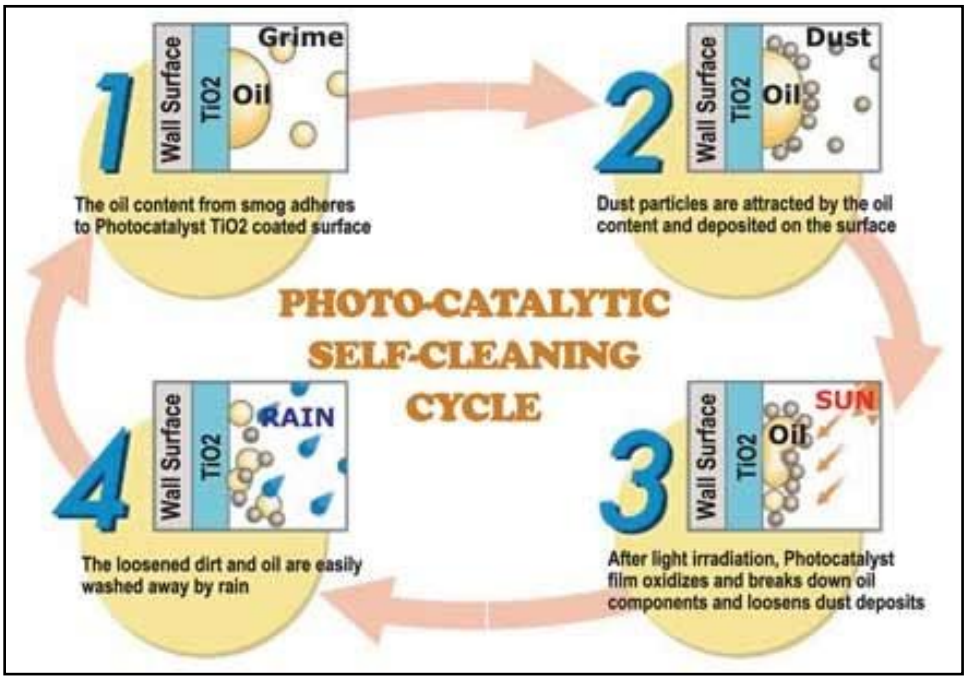

Fig.1.3 Photo-catalytic self cleaning cycle of TiO_2 [13]

1.2.4 Need of TiO_2 nanoparticles

- As the size of the TiO_2 particles decreases, the fraction of the atoms located at the surface increases with higher surface area to volume ratios, which can further **enhance the catalytic activity** [11].
- The increase in the band gap energy with decreasing nanoparticle size can potentially enhance the redox potential of the valence band holes and the conduction band electrons, allowing photo-redox reactions, which might not otherwise proceed in bulk materials, to occur readily.
- By a decrease in particle size below a certain limit, surface recombination processes became dominant. Since most of the electrons and holes were generated close to the surface and surface recombination was faster than interfacial charge carrier transfer processes.

1.2.5 Properties of TiO_2 nanoparticles

Thermodynamic properties: The crystal structure of TiO_2 nanoparticles depended largely on the preparation method. For small TiO_2 nanoparticles (<50 nm), anatase seemed more stable and transformed to rutile at >973 K. The transformation sequence and thermodynamic phase stability depended on the initial particle sizes of anatase. Only anatase to rutile phase transformation occurred in the temperature range of 973-1073 K.

Both anatase and rutile particle sizes increased with the increase of temperature, but the growth rate was different. Rutile had a much higher growth rate than anatase. The growth rate of anatase leveled off at 800 °C. Rutile particles, after nucleation, grew rapidly, whereas anatase particle size remained practically unchanged. With the decrease of initial particle size, the onset transition temperature was decreased [11]. The decreased thermal stability in finer nanoparticles was primarily due to the reduced activation energy as the size-related surface enthalpy and stress energy increased.

Electronic properties:

For nanoparticles, the band gap energy increases and the energy band becomes more discrete with decreasing size. As the size of a semiconductor nanoparticle falls below the Bohr radius of

the first excitation state or becomes comparable to the de Broglie wavelength of the charge carriers, the charge carriers begin to behave quantum mechanically and the charge confinement leads to a series of discrete electronic states [11]. However, there is a discrepancy in this critical size below which quantization effects are observed for TiO_2 nanomaterials with indirect band gaps. The estimated critical diameter depends critically on the effective masses of the charge carriers.

Optical properties: The main mechanism of light absorption in pure semiconductors is direct interband electron transitions. This absorption is especially small in indirect semiconductors, e.g. TiO_2, where the direct electron transitions between the band centers are prohibited by the crystal symmetry.

1.3 Glycolate route for the formation of TiO_2 nanoparticles

For a mono-disperse sample, the nucleation event must be well separated in time from the growth step, which generally means that nucleation must occur on a short time scale, of the order of a fraction of a second [15]. There are various methods in use for the synthesis of oxide nanopowders. We will be concentrating on the chemical synthesis methods because these methods help to achieve higher purity, better control of size and lower phase formation temperatures. One of the methods of oxide preperation is prepared via the glycolate route. This route involves preparation and subsequent calcination of Metal-glycolate. Formation of metal-glycolate generally involves heating of metal-alkoxide in excess of EG [17].

Advantages of Glycolate route

- The glycolate complexes are more resistant to hydrolysis, and could be kept in air for several months without observing any precipitation in the solution system.
- Nanostructures made of these glycolate precursors could not be dissolved using any known solvent. So, these complexes might also exist as relatively long chain polymers.
- This method provides larger scale of production, along with higher porosity and thus larger surface areas of nanostructures.

Importance of using EG as a reagent and reactive medium

1. EG has been widely used as a reagent due to its strong reducing power and relatively high boiling point (~197˚C) [17].
2. It serves as both a solvent as well as reagent and also as ligand to form bidentate chelate occupying sites on metal coordination spheres so as to bridge adjacent metal atoms [17].

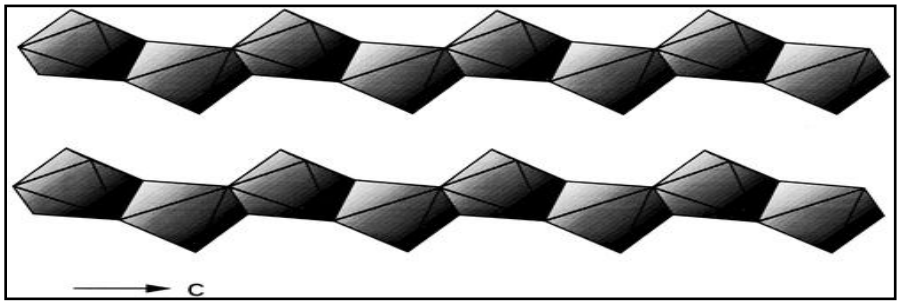

Fig.1.4 Polyhedral view of the 1-D chains of Ti $(OCH_2CH_2O)_2$ along the *c* axis [19].

Structure of TiG

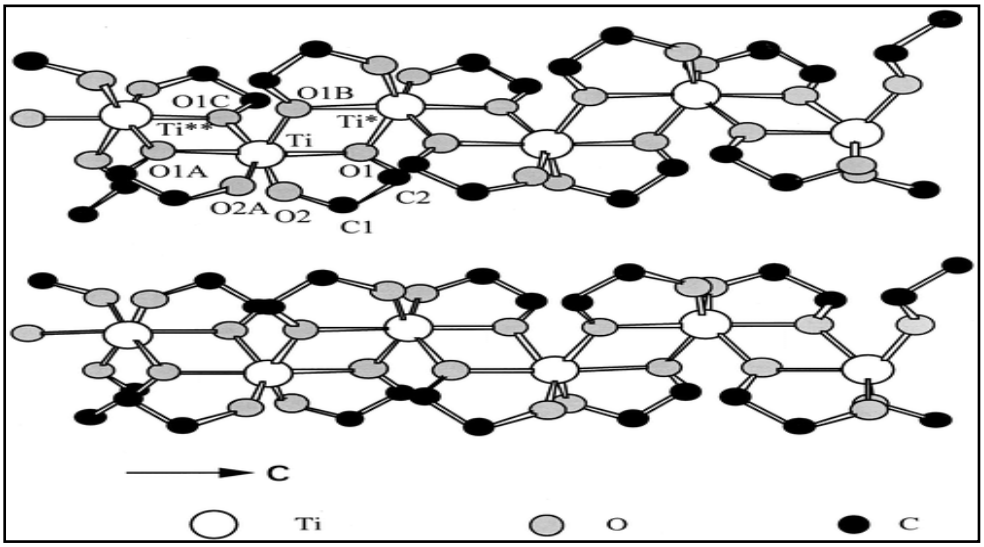

Fig.1.5 View of the 1-D chains of Ti $(OCH_2CH_2O)_2$ along the *c* axis [19]

$$Ti[O(CH_2)_3CH_3]_4 + HOCH_2CH_2OH \longrightarrow Ti[OHCH_2CH_2OH]_2 + H_2O$$

From the structure of TiG, we understand that both the Ti- but and EG have to be added in the molar ratio of 1:2 for the reaction to take place.

Since in the glycolate route EG acts both as reagent and solvent, therefore in the reaction mixture we always take excess of EG (> twice the number of moles of Ti- but).

When EG is used as a reactant for the formation of glycolate, we get very long 1-D structures (nano-wires). To limit the size we need capping agent.

Capping abilities of alcohol

During the synthesis, surface passivation helps to control the growth of the nanocrystal, prevents agglomeration and focusing of particles, and provides for the solubility of the nanocrystals in common solvents. Alcohol molecules are known to cap the surface of a glycolate[19]. Surface passivation can be achieved by using organic solvent or alcohol. So, alcohol used acts as solvent as well as capping agent.

Heat Treatment

Heat treatment is the process of heating the sample to a predetermined temperature, holding for a certain time, and then cooling to room temperature to improve its properties. Heat treatment is a method used to alter the physical, and chemical, properties of a material.

1.4 Literature review for the formation of TiO_2 via glycolate route:

Victor W. Day et.al. [16] reported the chemical synthesis of Ba-titanate obtained by calcinations of BTG. BTG could be prepared by reaction of EG and propanal with any of several barium reagents (BaO or Ba metal) and titanium(IV) reagents (TiO_2 or titanium isopropoxide) .

Precursors used**:** a) Barium oxide, BaO - 6.0 gm
b) EG - 30 ml
c) 2-Propanol - 40 ml
d) Titanium isopropoxide - 9.0

Molar ratio **:** Titanium isopropoxide: EG: 2-Propanol : : 1: 17.9: 17.4

Product obtained **:** Barium titanate powder with exaggerated grain diameters of 20 μm in a fine gain (0.5 μm) matrix were obtained.

Xuchuan Jiang, et.al. [17] demonstrated simple and convenient method for large-scale synthesis of metal oxide TiO_2 nanowires with diameters around 50 nm and lengths up to 30 mm. In a typical procedure, tetraalkoxyltitanium, $Ti(OR)_4$ (with R ~ $–C_2H_5$, –iso-C_3H_7, or –n-C_4H_9), was added to ethylene glycol and heated to 170 °C for 2 h under vigorous stirring. The alkoxide was transformed into a chain-like, glycolate complex that subsequently crystallized into uniform nanowires. The nanowires could be readily collected as precipitates after the reaction solutions had been cooled down to room temperature. By calcining at elevated temperatures, each glycolate precursor could be transformed into the corresponding metal oxide without changing the wire-like morphology.

The nanowires described here were polycrystalline in structure and thus intrinsically larger surface areas.

Precursors **:** a) Ti-but - 0.050 ml, ~0.147 mmol

b) EG - 10 ml

Molar ratio **:** Ti-but : EG : : 1 : 1220.5

Product obtained **:** Wire like nanostructure with typical diameters in the range 50 ± 8 nm were obtained.

Nuchnapa Tangboriboon, et.al. [18] reported an economical, simple and straightforward process for synthesizing highly moisture stable and pure metal alkoxide precursors using inexpensive and available starting materials. The reaction of lead acetate trihydrate ($Pb(CH_3COO)_2.3H_2O$), EG, using triethylenetetramine (TETA) as a catalyst, provides in one step access to a polymer-like precursor of lead glycolate which can be categorized as a condensation reaction generating water as a by-product.

Precursors **:** a) Lead acetate trihydrate - 0.1 mol, 37.9 gm

b) EG - 50 ml

c) TETA -14.6 gm

Molar ratio **:** Lead acetate: EG: TETA : : 1: 8.98: 1

$$Pb(CH_3COO)_2.3H_2O + HOCH_2CH_2OH \xrightarrow{\text{TETA , 200 °C}} -[-PbOCH_2CH_2O-]_n- + 3H_2O + 2CH_3COOH$$

XRD pattern gives an anatase phase at 500 ˚C to 900 ˚C and completely changes to rutile phase at 1100 ˚C upon calcination.

Product obtained**:** The light silver bronze solid powder was obtained.

Dan Wang, et.al. [19] Hydrothermally synthesized single crystals of a novel titanium glycolate complex, $Ti(OCH_2CH_2O)_2$. In this research, the crystallization of the product took advantage of the closed system and autogenous pressure, which are the characteristics of hydrothermal synthesis. Different from most crystalline titanium alkoxides, which are generally low polymeric molecules, $Ti(OCH_2CH_2O)_2$ is a novel crystalline complex with infinite one-dimensional chains. It exhibits outstanding high stability not only in alcohol but also in water.

Precursors **:** a) Tetraethyl orthotitanate, $Ti(OC_2H_5)_4$

b) n-Butylamine, $CH_3(CH_2)_3NH_2$

c) EG

Molar ratio **:** Tetraethyl orthotitanate: n-butylamine: EG : : 1 : 1 : 20

Product **:** Large transparent NEEDLE LIKE crystals upto several millimeters in length were obtained.

Yanting Li, et.al. [16] This paper presented an alcohothermal method for producing TiO_2 nanoparticles from $Ti(OC_4H_9^n)_4$ in 1-butanol medium. The obtained anatase TiO_2 nanoparticles show relatively high thermal stability and specific surface area after heat treatment.

Precursors **:** a) Tetra n-butyl titanate, $Ti(OC_4H_9^n)_4$

b) 1-Butanol, C_3H_8O

c) Concentrated HNO_3

d) Deionized water

Molar ratio **:** Tetra n-butyl titanate: 1-Butanol: conc.HNO_3: H_2O : : 1 : 0.19 : 55 : 1.5

Product obtained**:** Anatase TiO_2 POWDERS with high thermal stability, specific surface area and narrow pore distribution were obtained.

1.4 Organization of Thesis

The organization of the thesis is as follows:

Chapter 1 provides the introduction to the area.

Chapter 2 provides the details of experimental techniques used for the characterization of TiO_2.

Chapter 3 provides detailed method of preparation of TiO_2 samples

Chapter 4 provides the detailed thermal, optical and structural analysis of TiO_2 and TiG.

Chapter 5 provides conclusions of the thesis and scope for future work.

CHAPTER 2

EXPERIMENTAL TECHNIQUES

2.1 Optical Technique

2.1.1 FT-IR

The IR region comprises fundamental vibrations of bound atoms. Whenever such bound atoms vibrate, they absorb infrared energy i.e. they exhibit IR absorption bands [21].

There are two types of molecular vibrations:-

1. Stretching :-

   Stretching vibration is rhythmical movement along bond axis such that intermolecular distance either increases or decreases resulting in:

   a) Symmetrical stretching
   b) Asymmetrical stretching

(1) Symmetrical stretching (2) Asymmetrical stretching

Fig.2.1 Schematic representation of stretching of vibrational modes [21]

2. Bending :

   A bending vibration may consist of a change in bond angle between bonds with a common atom or the movement of a group of atoms with respect to the remainder of the molecule without movement of the atoms in the group with respect to one another.

   a) Twisting b) Rocking c) Torsional

(1) Out-of-plane bending or twisting (2) In-plane bending or rocking

Fig.2.2 Representation of bending of vibrational modes [21]

Conditions for IR spectroscopy

Only those vibrations that result in a rhythmical change in the dipole moment of the molecule are obtained in the IR. The symmetrical stretching vibrations are IR inactive since it produces no change in dipole moment of the molecule. Fundamental vibrations involve no change in the center of gravity of the molecule. The theoretical number of fundamental vibrations (absorption frequencies) are seldom be observed [22].

Instrumentation

FTIR working is based on MICHELSON INFEROMETER. Radiation containing all IR wavelengths (4000-400 cm^{-1}) is split into two beams. One beam is of fixed length, the other of variable length (moveable mirror). The varying distances between two path lengths result in a sequence of constructive and destructive interferences and hence variation on intensities: AN INTERFEROGRAM. Fourier transformation converts this interferogram from the time domain into one spectral point on the more familiar form of the frequency domain.

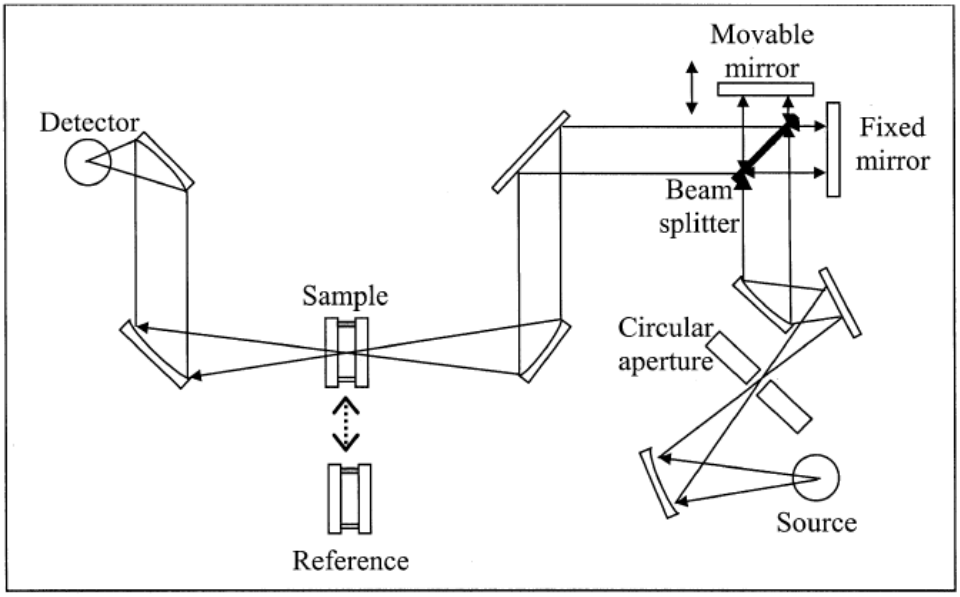

Fig.2.3 Diagram of FT-IR spectrometer with Michelson interferometer [22]

The mathematical procedure, which is employed to convert the IR interferogram (intensity versus time, also called time domain) to an IR spectrum (intensity versus frequency, also called frequency domain), is called Fourier transformation. Sample and reference interferograms are

separately transformed. Afterwards, the ratio of both is automatically calculated and displayed as instrument-independent IR transmission spectrum. Resolution in an FT-IR spectrometer is mainly defined by the maximum path difference between the interferometer arms [21].

Interpretation of spectra

- Many of the group absorptions vary over a wide range because the bands arise from complex interacting vibrations within a molecule.
- The two important areas for a preliminary examination of a spectrum are the regions 4000-1300 and 1300-900 cm^{-1}.
- The high frequency portion of the spectrum is called the functional group region. The characteristic stretching frequencies for important functional groups such as OH, NH and C=O occur in this portion of the spectrum. The absence of absorption in the assigned ranges for the various functional groups can usually be used as evidence for the absence of such groups in the molecule.
- The intermediate portion of the spectrum, 1300-900 cm^{-1}, is usually referred to as the 'FINGERPRINT' region. The absorption pattern in this region is frequently complex, with the bands originating in interacting vibrational modes. This portion of the spectrum is extremely valuable when examined in reference to the other regions.

2.2 Structural Techniques

2.2.1 XRD

Fundamental Principle

The phenomenon of diffraction is often associated with the bending of light at the corners or edges of aperture or an obstacle. A crystal is made up of families of lattice planes and that the scattering from a given family of planes will only be strong if the X-rays reflected by each plane arrive at the detector in phase [23].

The relationship between the X-ray wavelength λ, the spacing d between lattice planes and the angle of incidence θ is known as Bragg's law:

$$\lambda = 2d\sin\theta$$

The angle of deviation of the X-ray is 2θ from its initial direction. Analysis of the positions of the diffraction effect leads immediately to a knowledge of the size, shape and orientation of the unit cell. To locate the positions of the individual atoms in the cell, the intensities must be measured and analyzed.

X-ray diffraction (XRD) is a versatile, non-destructive technique that reveals detailed information about the chemical composition and crystallographic structure of natural and manufactured materials.

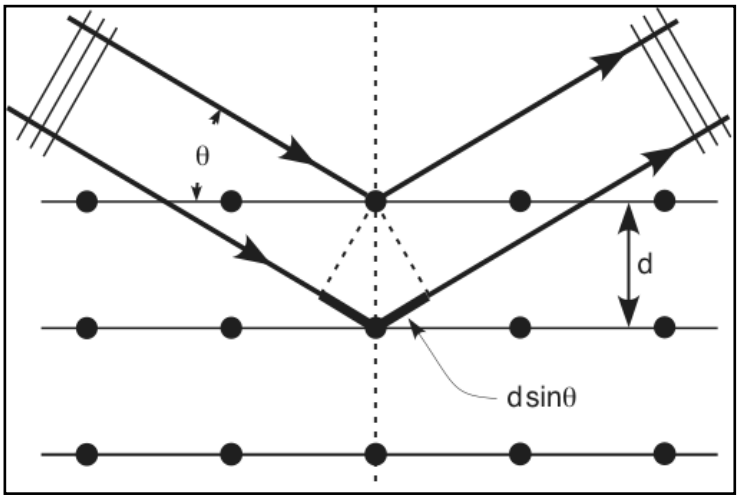

Fig.2.4 Schematic of Bragg's law [24]

Powder XRD

The essential feature of the powder diffraction technique include a narrow beam of monochromatic x-rays impinging upon a crystalline powder composed of fine, randomly oriented particles. The essence of this technique is to illuminate a large number of crystallites, so that a substantial number of them are in the correct orientation to diffract X-rays into the detector. Ideally, every possible crystalline orientation is represented equally in a powdered sample [25].

Advantages

The great advantages of the technique are:

• Simplicity of sample preparation

• The powder diffraction pattern is characterization of the substance.

- Each substance in a mixture produces its pattern independently of the others.
- The diffraction pattern indicates the states of chemical combination of the elements in the material.
- Only a minute amount of sample is required.
- The method is capable of measuring the average spacing between the layers or rows of atoms, the orientation of single crystal or grain, the size, shape and internal stress of small crystalline regions [14].

Particle size measurement

When the size of the individual crystals is less than about 0.1μm (1000Å), the term 'particle size' is usually used. Crystals in this size range cause broadening of the XRD peak.

$$T = 0.9\ \lambda/\beta\ \cos\theta$$

T = Crystallite size

β = Broadening of diffraction line measured at half its maximum intensity (radians)

All the diffraction lines have a measurable breadth, even when the crystal size is less than 1000Å, which is caused by the divergence of the incident beam, size of the sample and width of the x-ray source. The breadth β refers to broadening, due to particle size effect alone [26].

Let β_a be the measured breadth of bulk material at half maximum intensity.

β_o be the measured breadth of observed material at half maxima.

$$\beta = (\beta_o^2 - \beta_a^2)^{1/2}$$

Once β has been obtained, particle size distribution can be found by calculating T corresponding to three maximum peaks in XRD pattern obtained.

Unit Cell size determination

Anatase and Rutile phase of Titania (TiO_2) has tetragonal crystal structure [11], hence, $a = b \neq c$ and $\alpha = \beta = \gamma = 90°$.

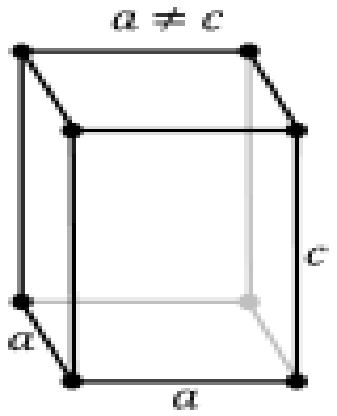

Fig.2.5 The unit cell of a tetragonal crystal [27]

For tetragonal structure, the interplanar spacing between the two closest parallel planes with the miller indices d_{hkl} , is given by [26]

$$\frac{1}{d^2} = \frac{h^2 + k^2}{a^2} + \frac{l^2}{c^2} = \frac{4\ sin^2\theta}{\lambda^2}$$

Where d_{hkl} = interplanar spacing or d-spacing

a, c = lattice constant (edge of unit cell)

h,k,l = Miller indices of planes being considered

Using above method, d-spacing, lattice parameters can be calculated provided all other parameters are known.

2.2.2 TEM

An electron microscope is a microscope that uses a beam of electrons to illuminate a specimen and create a highly magnified image. Electron microscopes have much greater resolution power than optical microscopes and can obtain much higher magnifications of up to 2 million times. The greater resolution and magnification of the electron microscope is due to the fact that the De Broglie wavelength of an electron is much smaller than that of a photon of visible light. The strength of electron technique lies in the fact that the electrons can be focused using electromagnetic lenses. Because of this reason high resolution images as well as diffracted pattern can be obtained from specific regions.

Transmission Electron Microscopy (TEM) is an electron microscopy technique in which the beams of electrons are transmitted through a thin specimen. TEM gives high resolution inner view of the materials. The variation in electron intensity across the specimen can also be used to image strain fields, defects and atomic columns [28].

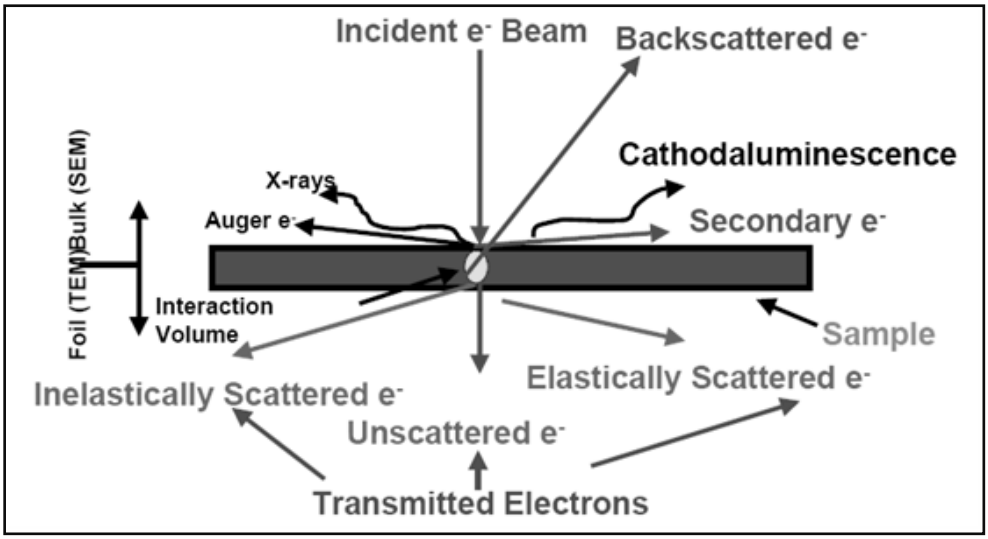

Fig.2.6 Schematic showing all possible electron sample interactions

Different imaging modes in TEM are:

- Bright Field Imaging
- Convergent Beam Electron Diffraction.
- Dark Field Imaging.
- Hi-Resolution Imaging.
- Selected Area Electron Diffraction.

Bright field imaging

This imaging mode in TEM uses intensity of the unscattered electrons i.e transmitted beam to form the image. Contrast in such an image is entirely due to thickness and density variations in the sample.

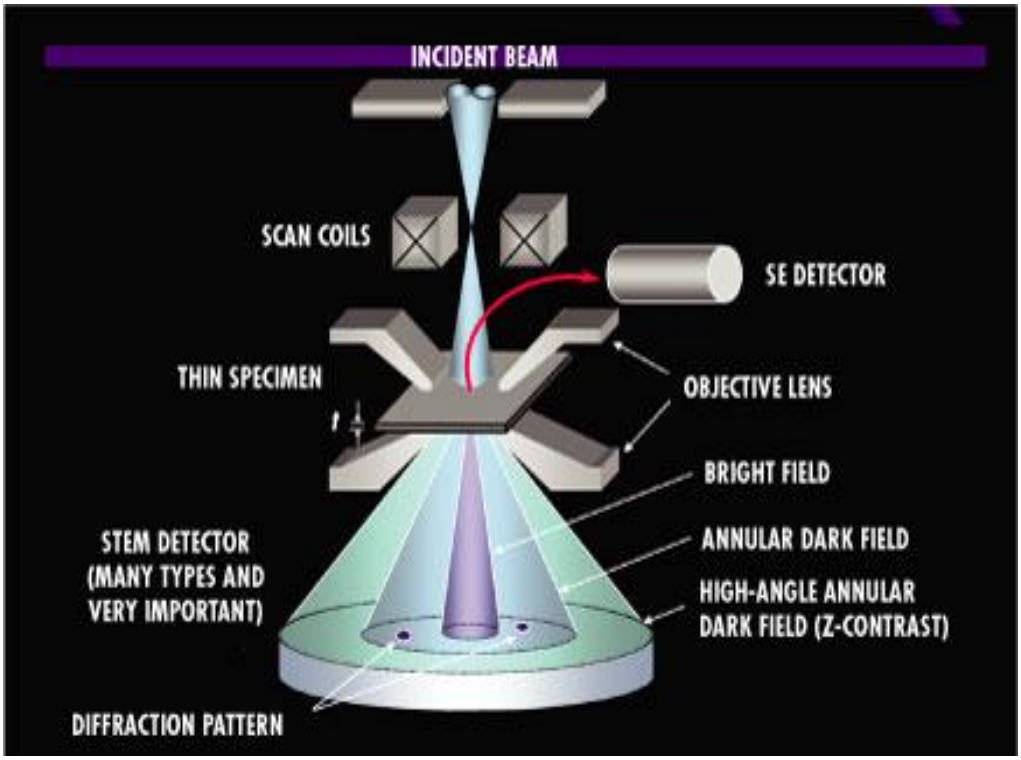

Fig.2.7 Bright field imaging in TEM [29]

In TEM, by adjusting the electron lenses, both the microscope images and diffraction patterns can be observed. By passing the transmitted beam or one of the diffracted beams through an aperture and changing to the imaging mode, the image with enhanced contrast can be observed.

2.3 THERMAL TECHNIQUES

2.3.1 DTA

DTA is a thermoanalytic technique. In DTA, the material under study and an inert reference are made to undergo identical thermal cycles, while recording any temperature difference between sample and reference. This differential temperature is then plotted against time, or against temperature (DTA curve or thermogram). Changes in the sample, either exothermic or endothermic, can be detected relative to the inert reference. Thus, a DTA curve provides data on the transformations that have occurred, such as glass transitions, crystallization, melting and sublimation. The area under a DTA peak is the enthalpy change and is not affected by the heat capacity of the sample [30].

The DTA Curve: A simple DTA curve may consist of linear portions displaced from the abscissa because the heat capacities and thermal conductivities of the test and reference samples are not identical, and it may also consist of the peaks corresponding to the evolution or absorption of heat following physical or chemical changes in test sample. The result of DTA experiment is a curve of differential temperature (heat flow) versus temperature or versus time. The convention generally adopted during the experiment is that the endothermic peak is taken to be negative.

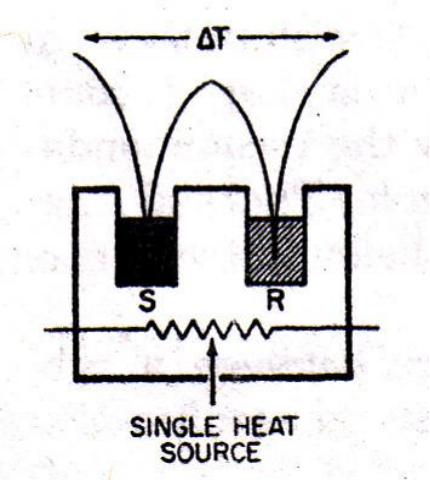

Fig.2.8 Schematic illustration of DTA set up

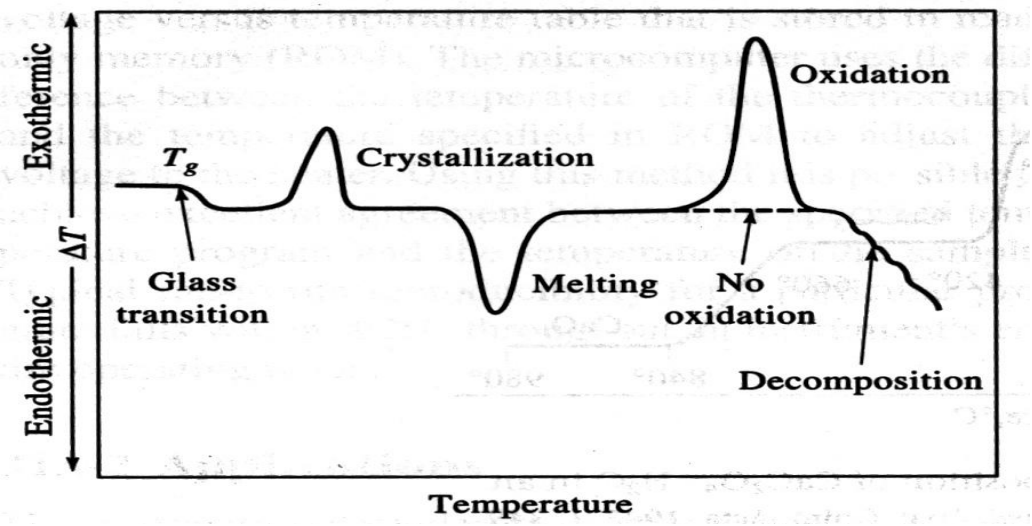

Fig.2.9 Schematic of all possible transitions in DTA

Interpretation of data

Fig. 2.9 gives the schematic of all possible transitions in a DTA [31]**.** The onset of the DTA peak in principle gives the starting temperature, but there may be temperature lags depending on the location of the thermocouple with respect to the reference and the test sample. It is wise to calibrate the apparatus with materials of precisely known melting points.

Melting

Melting is change from solid to liquid state. It is accompanied by an endothermic enthalpy change. Melting curves obtained in DTA depend on the purity and crystallanity of the sample, the thermal resistance, R_0, between the sample pan and the sample holder and the rate of change of temperature for the given programme [32].

Methodology for the determination of melting point: For a given instrument the thermal resistance R_0 is always constant. From the curve of fusion of an ultra pure metal the leading edge of the peak is extrapolated downwards and its intersection with the baseline is defined as the onset temperature (Fig. 2.8).

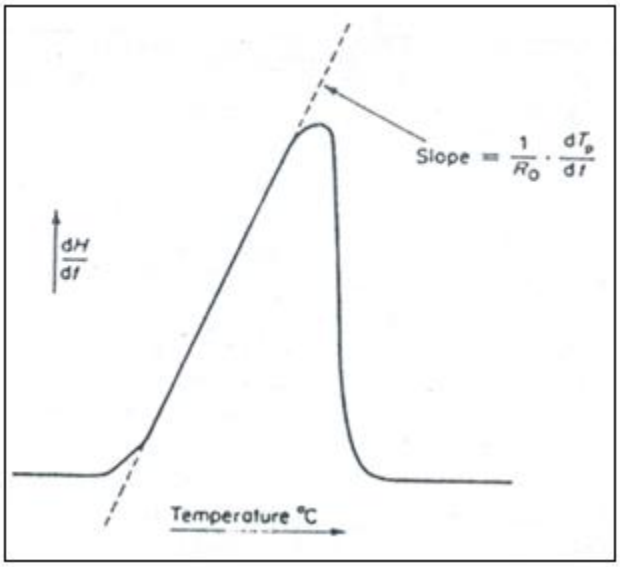

Fig.2.10 Thermogram for the fusion of 99.99% pure metal [32].

The true melting temperature of any other sample is determined as an extrapolated onset temperature using the slope determined with the ultrapure metal. (Fig.2.8)

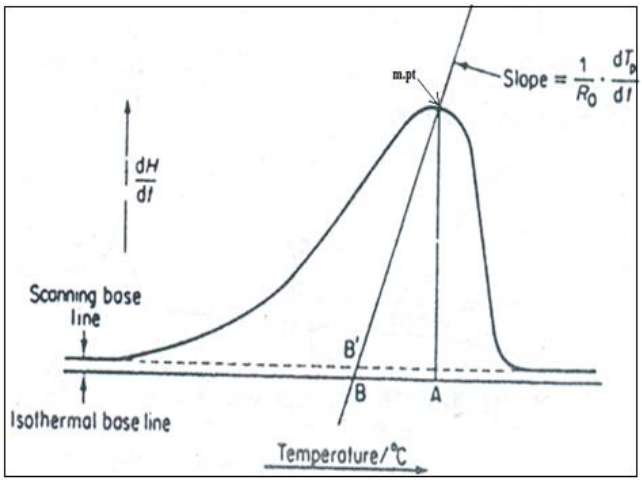

Fig.2.11 Details of the onset temperature determination for a given sample in a DTA [32].

Steps involved:

- Determine the leading edge slope for a standard ultrapure metal at the same heating rate as to be used for the sample
- For the DTA curve of the sample draw the base line.
- Determine the point of intersection with the extrapolated leading edge slope passing through the apex of the curve.
- This is the onset temperature for a given transition and for the melting transitions it is called the melting point.

Crystallization

The cooling curve crystallization (exothermic) characterizes the change in enthalpy when a material in the amorphous state is transformed into a solid crystalline state, as the temperature decreases.

The cooling rate determines the position of the crystallization curve on the temperature scale. As the cooling rate increases, the crystallization curve is displaced toward lower temperatures. Crystallization can be measured not only during cooling but also during heating and is called **cold crystallization**. It can occur if the material is quenched from the melt without allowing the crystallization to occur or for the case of protein/organic capping mediated precipitation of a material. Crystallization point can be determined in the same way as the melting point [32].

2.3.2 TGA

Thermogravimetric analysis (TGA) is used to measure the mass or change in mass of a sample as a function of temperature or time or both. Change of mass occurs during sublimation, evaporation, decomposition, chemical reaction, and magnetic or electrical transformation [14]. Crucial factors are the choice of purge gas and the conditions present in the specimen chamber. The purge gases consist of inert or oxidizing gases, such as nitrogen, helium, argon and oxygen, or air. The extent of heat transfer to the specimen depends on the gas flow rate. TGA is a type of testing that is performed on samples to determine changes in weight in relation to change in temperature. Such analysis relies on a high degree of precision in three measurements: weight, temperature, and temperature change.

In dynamic measurements, the starting temperature is generally room temperature and the final temperature around 1000˚C. The heating rate has a major effect on the results [32].

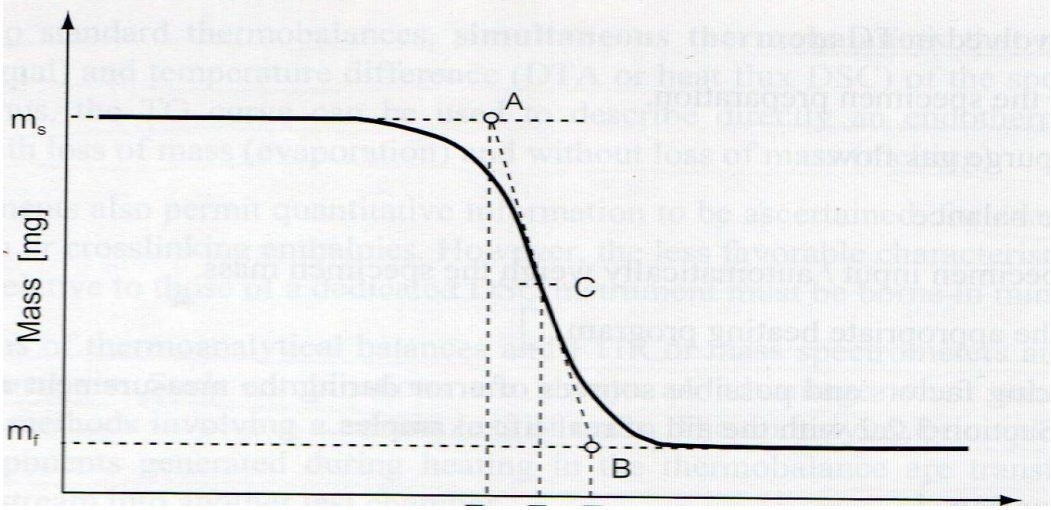

Fig.2.12 Schematic of transitions in TGA

CHAPTER 3

SAMPLE

PREPARATION

3.1 Chemicals used

Titanium(IV) Butoxide [33], Ethylene Glycol (EG) [34], tertiary-Butanol [35] and Ethanol [36]. All the chemicals and reagents were used as-received and are of AR grade.

3.2 Preparation

1. Ti-but was added to a round bottle flask containing EG and tert-Butanol in different sets of molar ratios (table given below) to form a uniform mixture.

S.No	SAMPLE NAME	MOLAR RATIO Ti-but : EG : tert-Butanol
1.	L2	1 : 70 : 70
2.	L3	1 : 70 : 30
3.	L4	1 : 72 : 0
4.	L5	1 : 70 : 2
5.	L6	1 : 20 : 1
6.	L7	1 : 1000: 0

Table 3.1 Samples names for different molar ratios

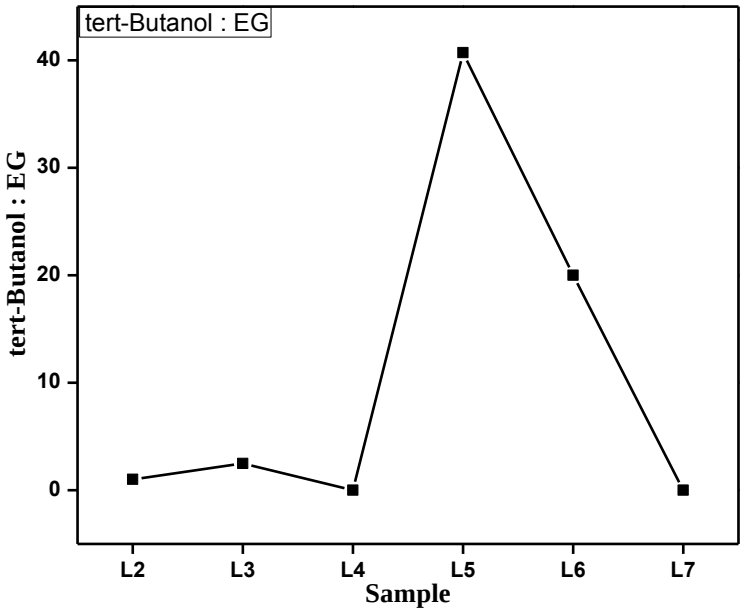

Fig.3.1 Graph showing variation of tert-Butanol : EG in each sample

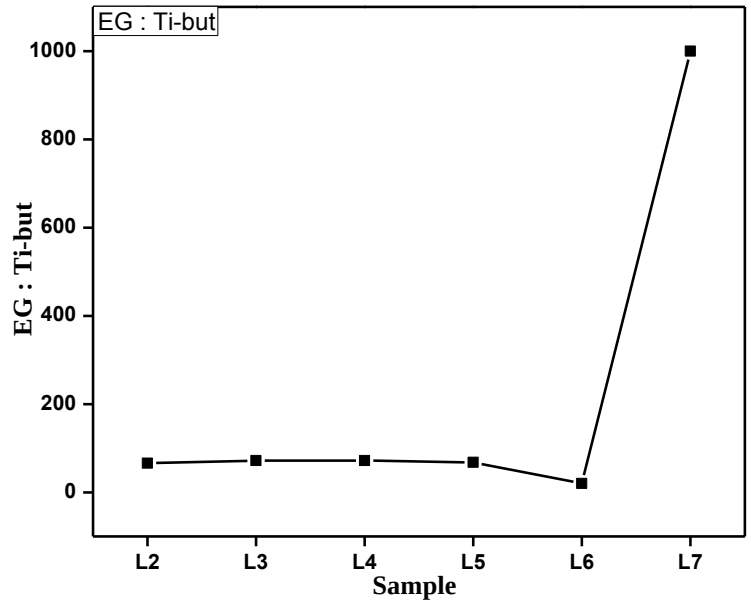

Fig.3.2 Graph showing variation of EG : Ti-but in each sample

2. The solution was mixed under constant magnetic stirring for ½ hr.
3. The mixture was then heated upto and maintained at 160 ^{o}C using oil bath under continuous magnetic stirring for 2 hrs. During this process, nucleation and growth of TiG happens.
4. After cooling down to room temperature for 1 hr, the white flocculate was harvested using centrifugation at 1800 rpm, followed by washing with ethanol for 3-4 times to remove excess of EG from sample.
5. The precipitates were finally dried in a vacuum oven at 50 ^{o}C for 2 hrs.

3.3 Heat Treatment

TiG powder obtained was converted to TiO_2 by calcinations i.e. heating the sample in air for different temperatures. The maximum temperature attained for calcination was 850 ^{0}C.

CHAPTER 4

EXPERIMENTAL ANALYSIS

4.1 SAMPLE PREPARATION AND INSTRUMENTATION FOR CHARACTERIZATION TECHNIQUES

- **XRD** data was acquired for powder samples using a Rigaku pro analytical X-ray diffractometer using Cu K_α radiation (λ = 1.54060Å) with the scanning rate of 0.0130° for 2θ in the range of 5 to 80°. Peak analysis was done using PowderX software.

- **FT-IR** spectra was acquired under ambient conditions using Perkin Elmer Spectrum BX in the range 4000-400 cm^{-1} and resolution of 2 cm^{-1}. The TiG samples were dispersed in ethanol and the calcined TiO_2 powder was used in pellet form.

- **TGA** and **DTA** was carried out in a Perkin Elmer Diamond TGA/DTA system using TiG powder (dried for 2 hrs at 50 ^oC) over a temperature range of 50 ^oC-900 °C at the rate of 10 °C/min. Argon was purged to create an inert atmosphere through the system.

- **TEM** images were taken using Hitachi 7500 machine operated at 80kV with a resolution of 2Å. The sample was prepared by placing one drop of the dilute water suspension on a carbon coated TEM grid, and letting the solvent evaporate slowly.

4.2 EXPERIMENTAL DETAILS

4.2.1 TGA Analysis

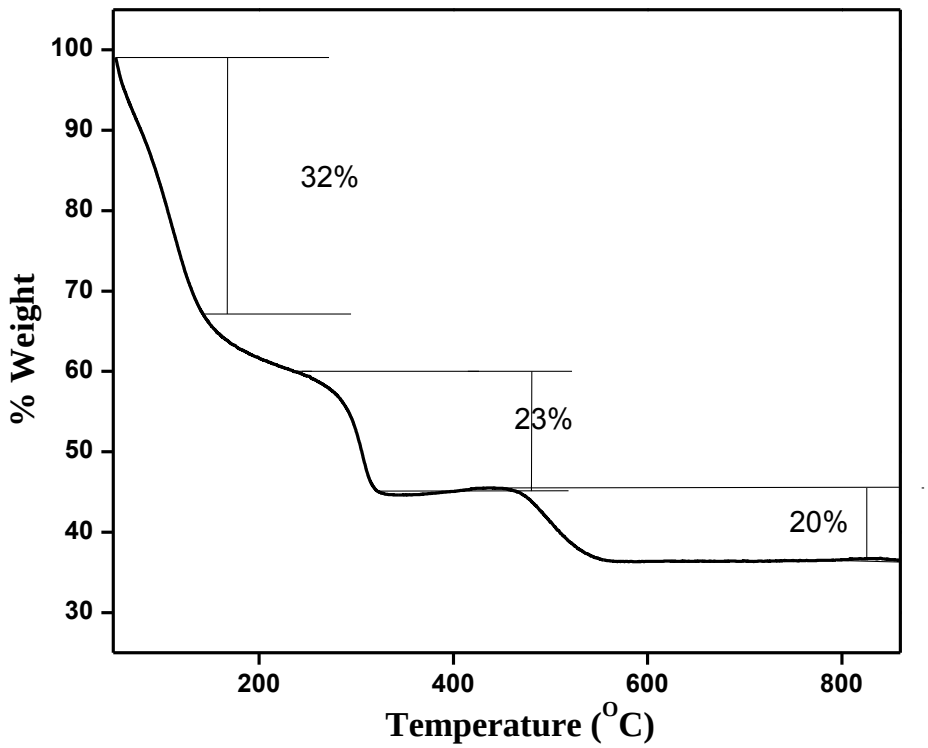

Fig.4.1 TGA curve of TiG

Fig.4.1 shows a typical TGA curve obtained for the TiG samples, indicating an initial continuous mass loss followed by a two-step weight loss.

Data Analysis

- Continuous mass loss (32%) within 150 ^{o}C is due to the loss of physically adsorbed water molecules as well as loss of volatile impurities present if any.
- In the first step the weight loss of 23% is due to evaporation of EG molecules in the temperature range of 240 to 325 ℃ [16].
- Weight loss of 20% in the temperature range of 445 to 575 ℃ is attributed to conversion of glycolate ligands into oxide ligands.

These results are consistent with the calculated value for all organic groups separating themselves from the framework [16, 37].

4.2.2. DTA Analysis

Fig.4.2 shows the typical DTA curve obtained for the TiG samples. The DTA curve shows two sharp exothermic peaks and one very small peak ~800 ^{o}C. Using the method mentioned in chapter 2 we have determined the various transition temperatures Fig.4.4.

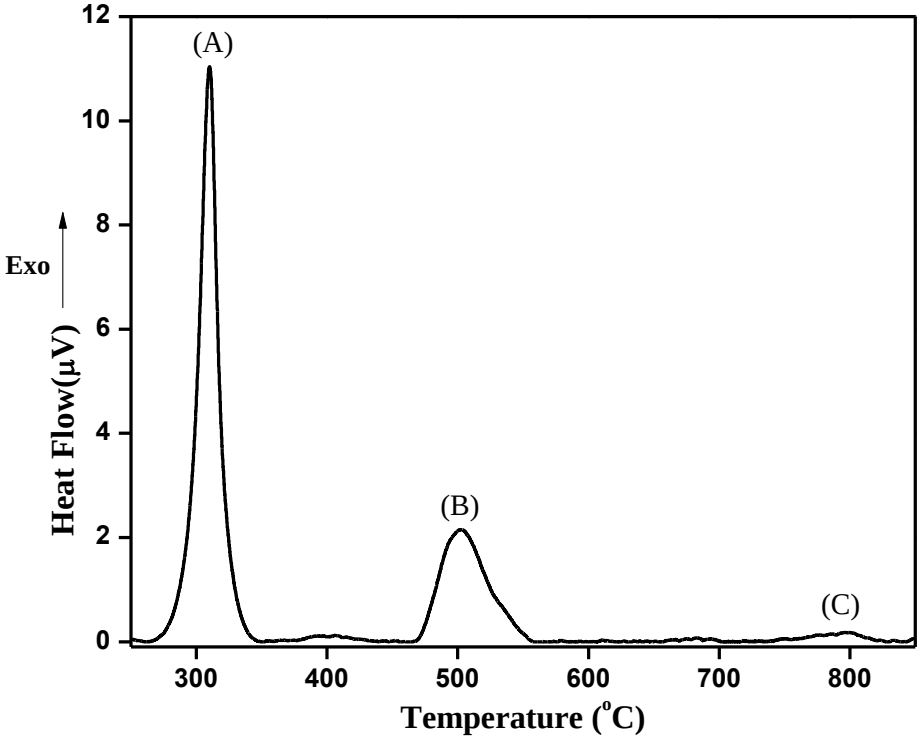

Fig.4.2 DTA plot (baseline removed) of TiG

The onset temperatures for the transitions were calculated using standard DTA curve for the fusion of 99.9% pure Tin. Slope of curve shown above in Fig.4.3 was used for the calculations.

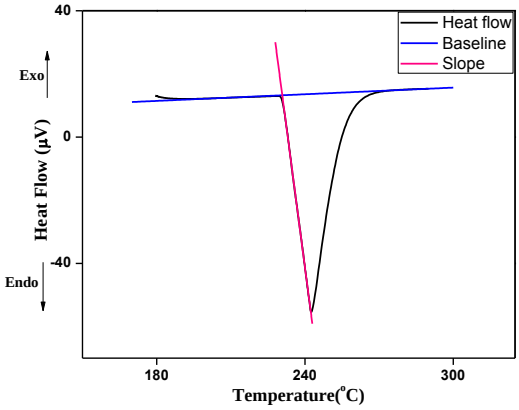

Fig.4.3 DTA plot for the fusion of 99.9% pure Tin

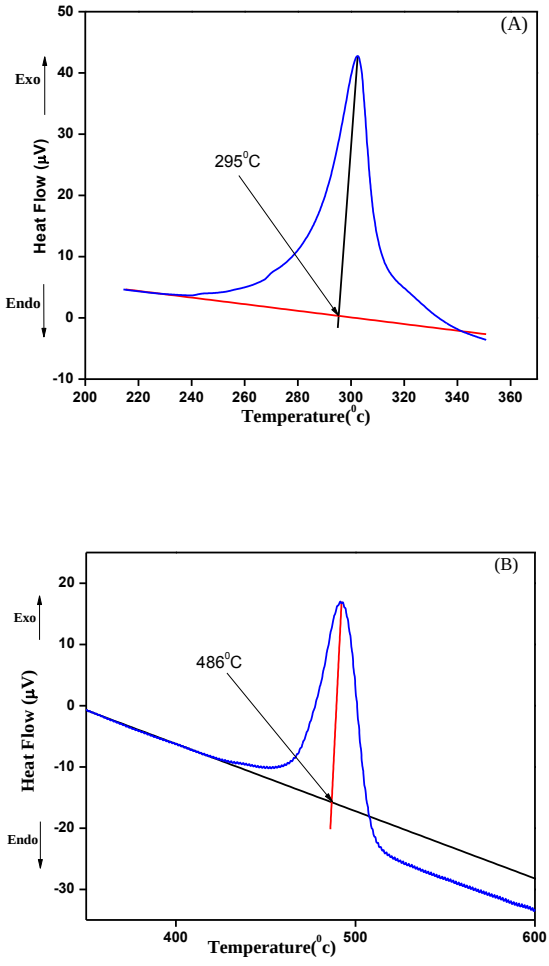

Fig.4.4 Transition temperature analysis of exothermic peaks (A) and (B) in DTA of TiG

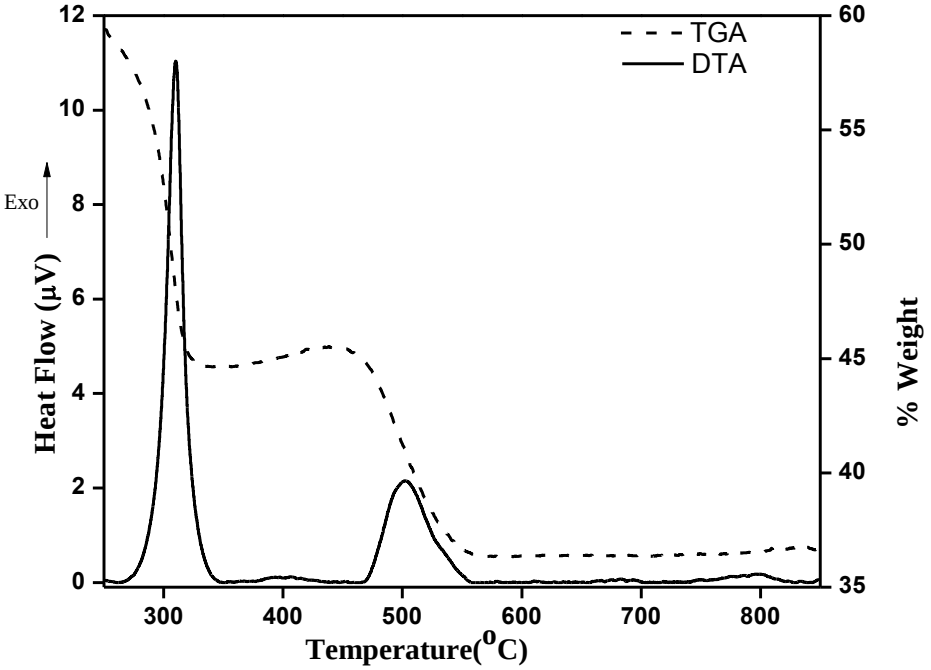

Fig.4.5 Combined graph of DTA and TGA for TiG

Data analysis for DTA data:

A) The transition onset temperature for the transition peak A is 295 ^{o}C and that for the transition leading to peak B is 486 ^{o}C. The C transition is very weak so we have not determined the exact onset temperature.

B) Comparing the TGA and DTA curves in the relevant temperature range (Fig.4.5) leads to the following conclusions:

   i) Peak A in DTA is associated with the first step in the two step mass loss observed in TGA and corresponds to loss of organic molecules especially EG via conversion into CO_2 and H_2O [19].

   ii) Peak B in DTA is associated with the second step in the two step mass loss observed in TGA and corresponds to loss of glycolate ligands and conversion from amorphous phase to crystalline phase. The last conclusion will need to be checked by XRD [19].

   iii) Peak C is a very weak and is not associated with any mass loss.

4.2.3 FT-IR Analysis

FT-IR spectrum of as prepared samples of TiG and crystalline phase (heated at 500 ˚C) are shown in figure below.

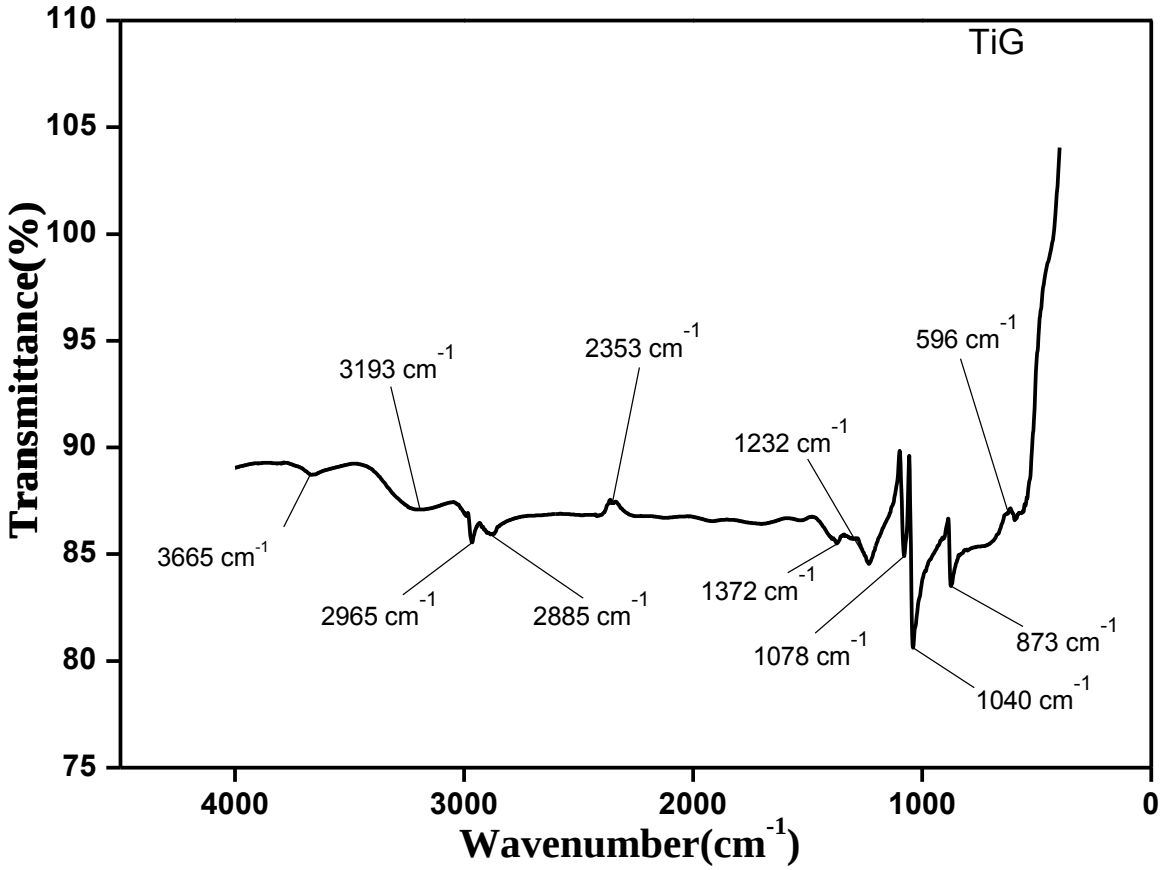

Fig.4.6 FT-IR data for TiG

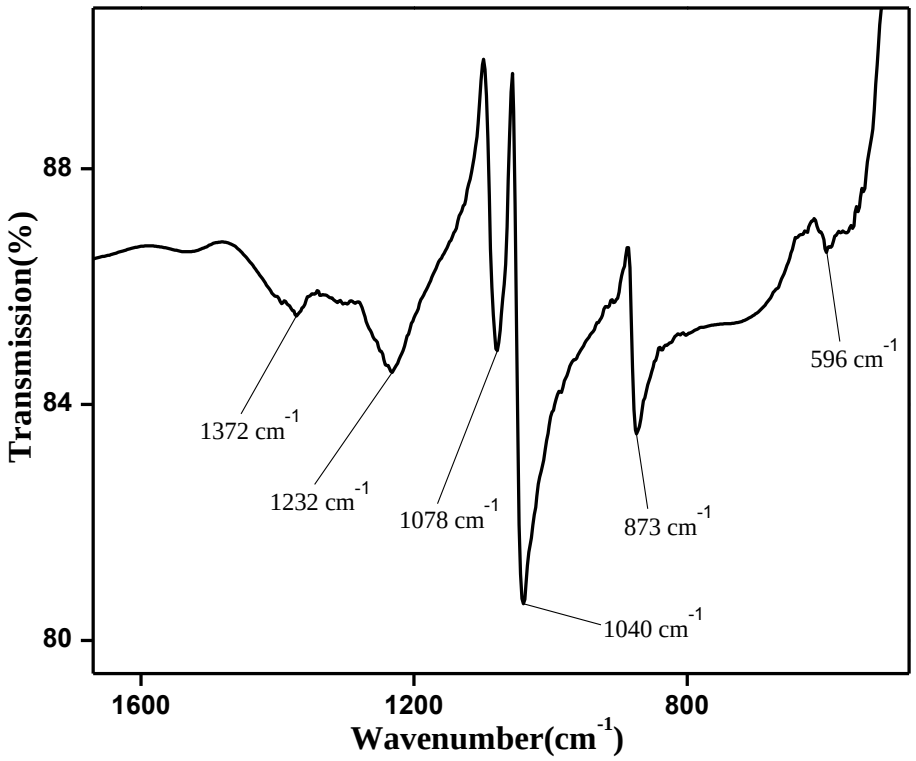

Fig.4.7 Inset of FT-IR for TiG showing region in the range 1232 – 624 cm^{-1}

Data analysis for TiG in FT-IR curve (Fig.4.6):

- The characteristic bands at 3665 and 3193 cm^{-1} correspond to hydroxyl group (-OH bond) which are ascribed to the atmospheric water/ethanol used during washing in the synthesis process [17].
- The absorption bands occurring at 2965-2885, 1372 cm^{-1} corresponds to C-H stretching of an ethylene glycol ligand [36]
- The absorption bands 1232-1040 cm^{-1} corresponds to asymmetric/symmetric stretching vibration of carbonyl group (C=O) respectively [20].
- The band located at 1078 and 873 cm^{-1} indicates the presence of Ti-O-C linkage [19].
- The peak at 596 cm^{-1} is due to presence of Ti-O bond [17].

The last two peaks confirm the formation of the TiG in our experiment.

Data analysis for Crystalline (500 ^{o}C) phase of TiO_2 in FT-IR curve (Fig.4.7):

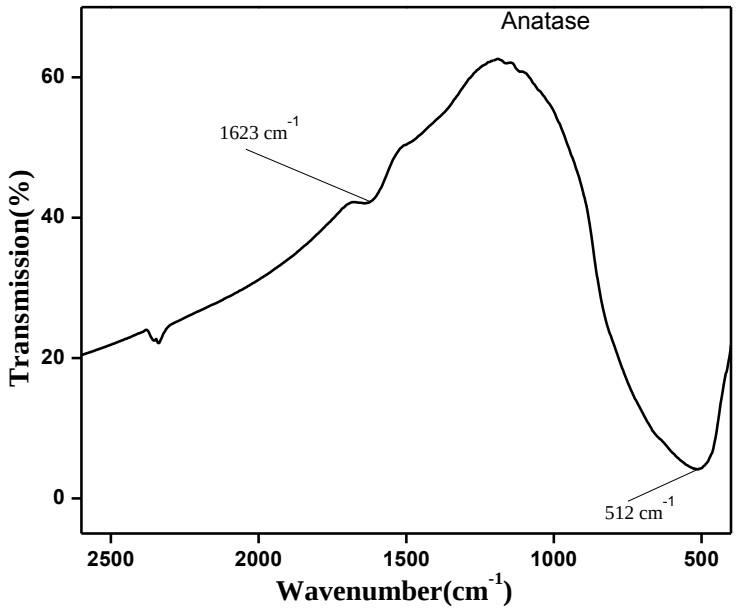

Fig.4.8 FT-IR data for anatase phase of TiO_2

- Thermal treatment at high temperature is accompanied with the decomposition of surface alkoxy groups and disappearance of the corresponding bands from the absorption spectrum.
- As the temperature was increased to 500 °C, the bands corresponding to physically absorbed water (-OH bond) also disappeared [17].
- A band at 1623 cm^{-1} which is absent in TiG (attributed to deformation vibrations of molecular water) shows that the TiO_2 particles calcined at high temperature are in favor of water adsorption onto the surface. These are visible since the FTIR is done at room temperature in ambient conditions [20].
- Once the amorphous structure has been transformed into the anatase phase of TiO_2, the Ti-O stretching band shifted from 596 cm^{-1} to higher wavelength i.e. ~512 cm^{-1}.

These results are consistent with the standard results [17].

4.2.4 XRD Analysis

The typical XRD peaks for the different TiG samples heated to 500 ^{o}C and 850 ^{o}C are shown in Fig.4.8. The samples which were heated to 350 ^{o}C were amorphous in nature.

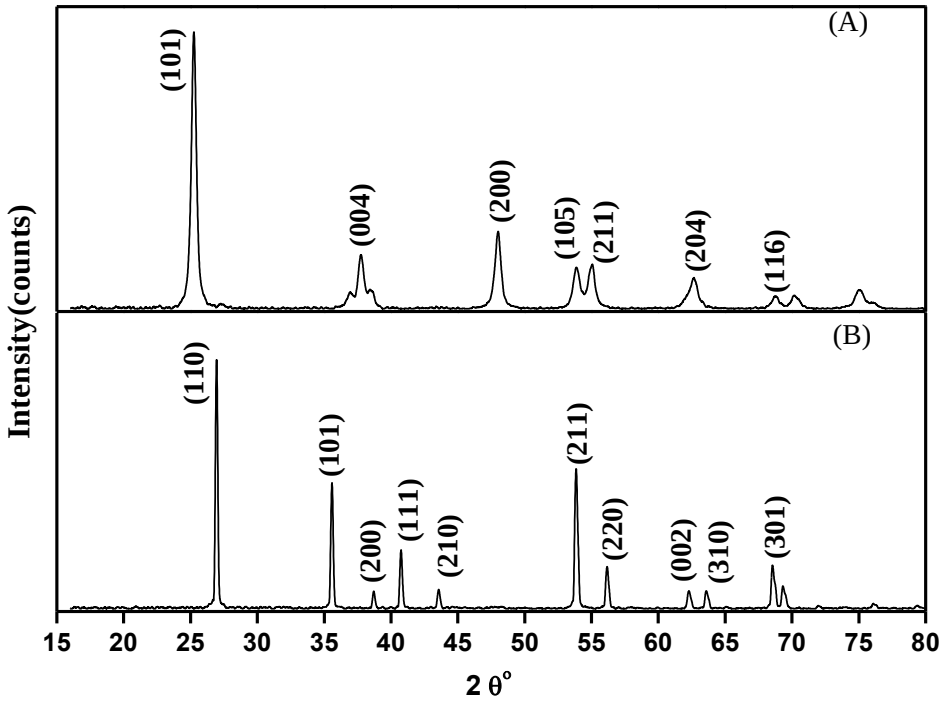

Fig.4.9 XRD patterns for the TiG samples heated at (A) 500 ^{o}C and (B) 850 ^{o}C

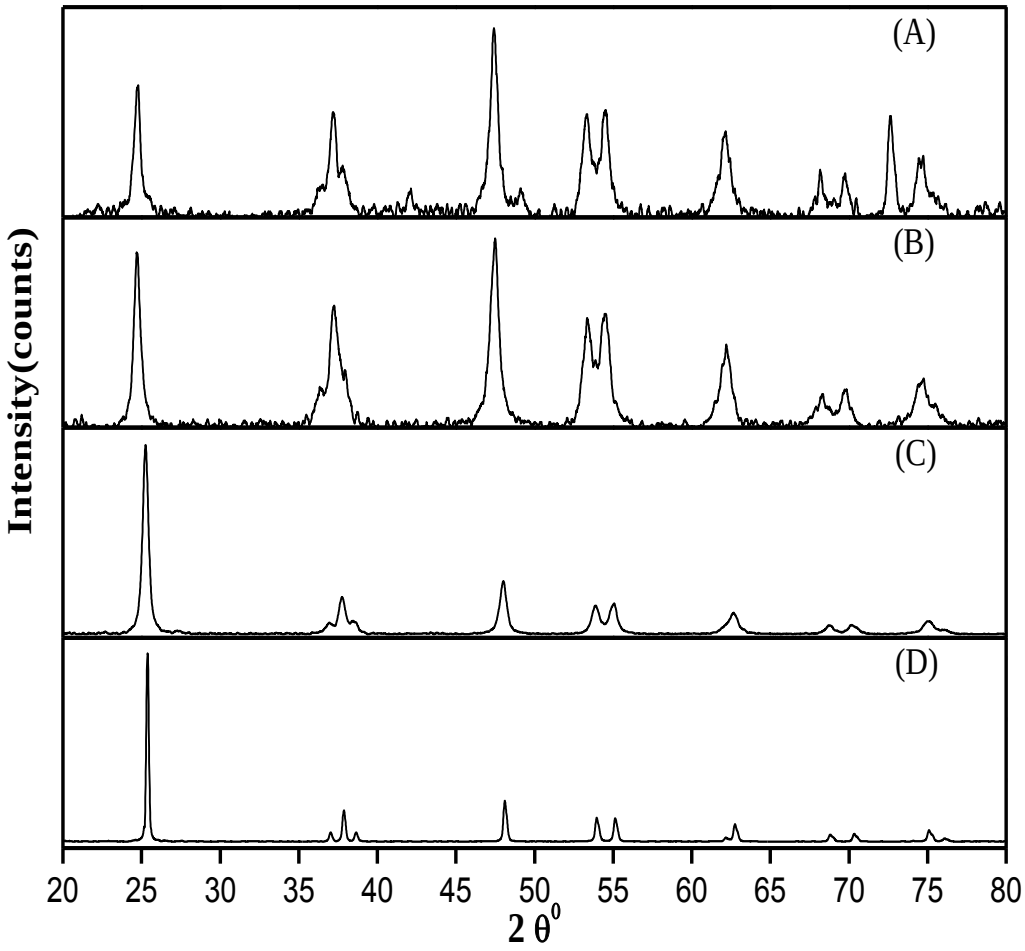

Fig.4.10 XRD pattern of 500 ^{o}C crystalline phase of TiO_2 A) L4 B) L5 C) L7 and D) bulk TiO_2

Data Analysis for XRD data:

- The diffraction peaks positioned at [101], [200], [105] and [211] crystal planes in all the 500 ˚C samples and at [110], [101], [111] and [211] in 850 ˚C samples have high intensity (Fig. 4.8). These peaks are in good agreement with the standard results of Anatase phase (PCPDF file no.78-2486) and Rutile phase (PCPDF file no. 76-0326) of TiO_2 respectively.

- The XRD data peak positions are same for all the samples heated to a given temperature (Fig. 4.10).
- The phases formed are pure.
- All the samples show marked peak broadening confirming that the samples are indeed nanostructures. The size analysis has been done.
- Different samples have different broadening.

Particle Size Analysis

Formula Used

Average crystallite size has been calculated from the recorded XRD pattern using well known Debye Scherrer Equation

$$T = \frac{0.9\,\lambda}{\cos\,\theta\,\sqrt{\beta_s{}^2 - \beta_b{}^2}}$$

Where $\lambda = 1.54060$ Å

β_s = F.W.H.M of sample in radians

β_b = F.W.H.M of bulk material in radians

θ = Position corresponding to a peak

S.No.	SAMPLE NAME	PARTICLE SIZE
1.	L2 500	27 nm
2.	L3 500	27 nm
3.	L4 500	30 nm
4.	L5 500	26 nm
5.	L6 500	27 nm
6.	L7 500	30 nm

Table 4.1 Calculated crystallite size of anatase phase in different samples

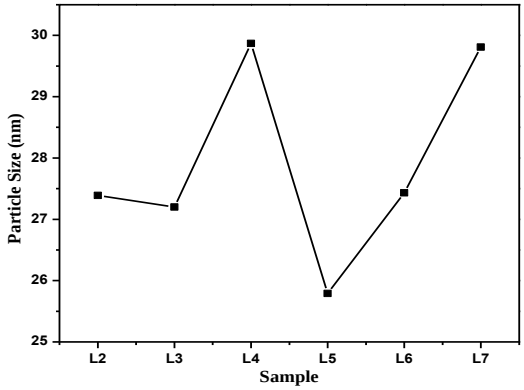

Fig.4.11 Graph showing variation of anatase phase TiO_2 crystallite size in each sample

Unit cell determination

For tetragonal structure, the interplanar spacing between the two closest parallel planes with the miller indices d_{hkl}, is given by [26]

$$\frac{1}{d^2} = \frac{h^2 + k^2}{a^2} + \frac{l^2}{c^2} = \frac{4\ sin^2\theta}{\lambda^2}$$

Using above formula, the calculated values of lattice parameters a, c

Lattice Parameters	Anatase	Rutile
a (Å)	3.812	4.651
c (Å)	9.603	2.979

Table 4.2 Lattice parameters of anatase and rutile phase of TiO_2 samples

The values obtained are in complete agreement with the standard value [11].

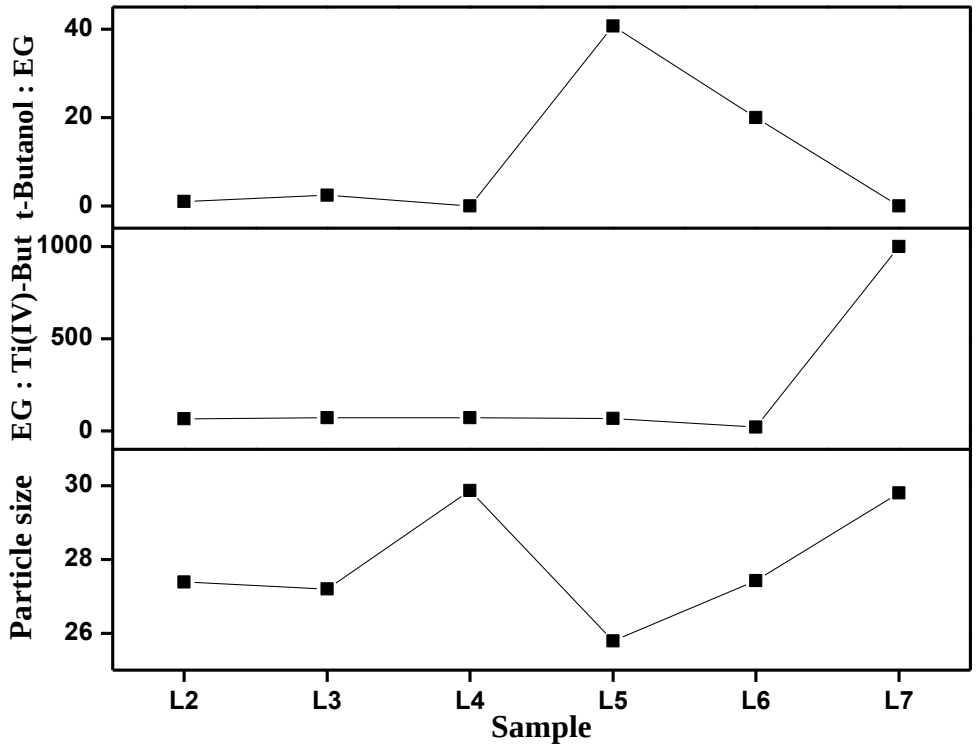

Fig.4.12 A combined graph showing the variation of size with change in the molar ratios of t-Butanol : EG and EG : Ti(IV)-But

The Fig.4.12 clearly indicates that the particle size has decreased as the ratio of t-butanol:EG increases. This is a confirmation of the capping properties of the t-butanol.

4.2.5. TEM Analysis

a) 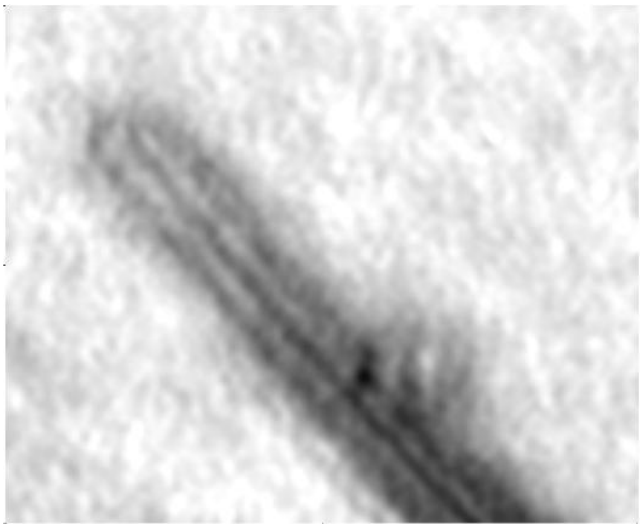 b) 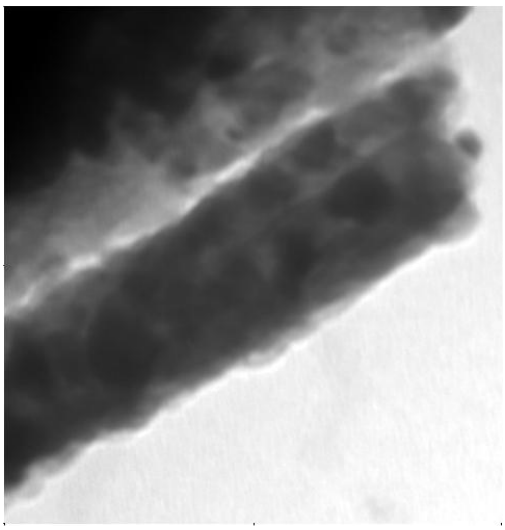

Fig. 4.13 TEM images of L7: a) Showing two nanorods (74 nm X 61 nm) b) Cluster of nanorods (150 nm X 143 nm

a) 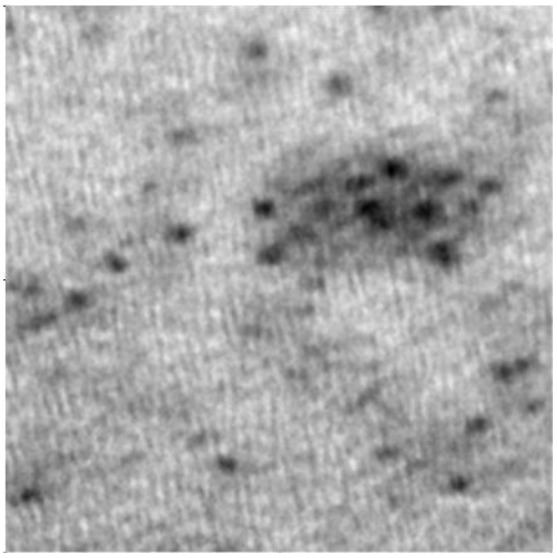 b) 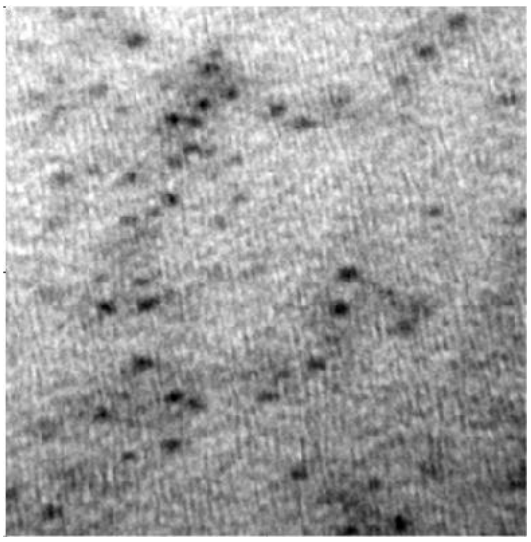

Fig. 4.14 TEM images of L5, cluster of particles: a) 65 nm X 65 nm b) 80 nm X 83 nm

a) 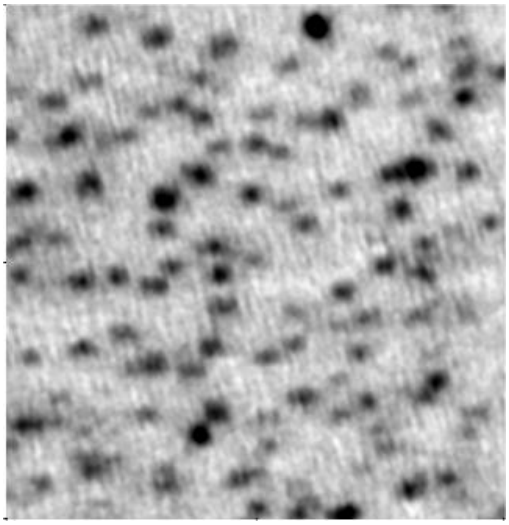 b) 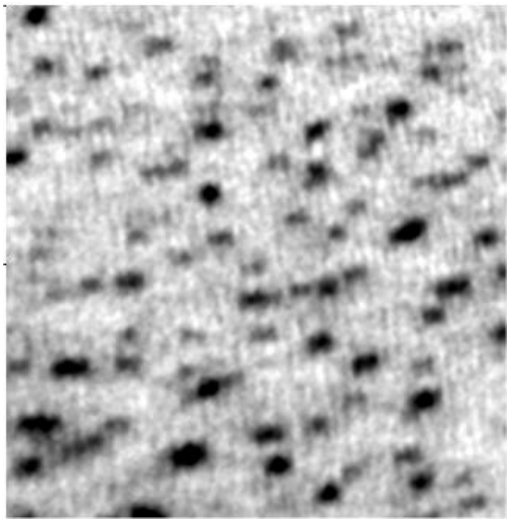

Fig. 4.15 TEM images of L4, clusters of particles: a) 80 nm X 83 nm b) 80 nm X 83 nm

Data analysis:

- The sample L7 with excess of EG shows rod like structures.
- The sample L5 in which the alcohol has been added shows spherical monodispersed particles.
- The sample L4 with no alcohol and less EG shows polydispersed paricles of no fixed shape.
- These results confirm our conjecture that alcohol can be used as a capping agent in the formation of monodispersed nanoparticles via the glycolate route.
- In the absence of alcohol (capping agent) the glycolate structures (which determine the morphology of the final nanoparticles) terminate at different sizes resulting in polydispersed particles (L4).

CHAPTER 5

CONCLUSIONS

5.1 CONCLUSIONS

The aim of the present work was to synthesize TiO_2 nanoparticles, using glycolate route and monitor the effect of alcohol as a capping agent and see its effects on particle morphology especially size. Titanium glycolate as well as TiO_2 particles formed were characterized optically (FT-IR), structurally (XRD, TEM) as well as thermally (DTA, TGA). After this study, we drive the following conclusions:

- The XRD analysis (peak positions, width analysis as well as the unit cell dimensions) shows that the particles formed have nano dimensions and are pure in crystalline phase as well as defect free.
- The crystallization temperature (the temperature at which amorphous Titanium glycolate undergo phase change to form crystalline phase) is 486 °C. And the Rutile phase is obtained by heating above 800 °C.
- The size of the particles has decreased as the ratio of t-Butanol : EG increased. This is a confirmation of the capping properties of the t-Butanol. Hence, t-Butanol can be used as a means of regulating the particle size in the formation of oxide nanoparticles via the glycolate route.

5.2 SCOPE FOR FUTURE WORK

This work can be further extended to see the effect of change in alcohol concentration on the particle morphology. The change in the carbon chain length and the position of hydroxyl group changes the hydrolyzing abilities of an alcohol and hence will modify its capping capabilities. So, the effects of different alcohols on the morphology should be interesting. The particles formed should be checked for photo-catalytic activity. Also, the band gap of these particles should be characterized using UV-Vis Spectroscopy and Photoluminescence.

CHAPTER 6

REFERENCES

6.1 References

1. National Nanotechnology Initiative 2000 leading to the next Industrial Revolution, A Report by the Interagency working group on Nanoscience, Engineering and Technology (http://www.nano.gov).
2. http://www.nanoed.org/lessons/Apples_to_Atoms/AtoAch5.pdf
3. http://www.evidenttech.com/quantum-dots-explained/quantum-dot-glossary.html
4. http://www.biologyjunction.com/images/clip01351.jpg
5. R. Rossetti, J.L. Ellison, J.M. Gibson, L.E. Brus, J. Chem. Phys. **80,** (1984) 4464.
6. W. Sang, Yo. Qian, J. Min, Do. Li, L. Wang, W. Shi, Yi. Liu, Solid State Commun **121**, (2002) 475.
7. A. P. Alivisatos, Science **271**, (1996) 933.
8. Singto Sakulkhaemaruethai, Sorapong Pavasupree, Yoshikazu Suzuki, Susumu Yoshikawa. Materials Letters **59**, (2005) 2965.
9. http://upload.wikimedia.org/wikipedia/commons/4/49/Anatase-unit-cell-3D-balls.png
10. http://image.absoluteastronomy.com/images/encyclopediaimages/r/ru/rutile-unit-cell-3d-balls.png
11. Xiaobo Chen and Samuel S. Mao. Chem. Rev. **107**, (2007) 2891.
12. www.almazoptics.com/**TiO2**
13. http://www.envirogta.com/images/solarstucco1.jpg
14. www.wikipedia.com
15. X. Peng, J. Wickham, A. P. Alivisatos, J. Am. Chem. Soc.**120**, (1998) 5343.
16. Victor W. Day, Todd A. Eberspacher Matthew H. Frey, W. G. Klemperer, Shurong Liang, and David A.Payne. Chem. Mater. **8**, (1996) 330.
17. Xuchuan Jiang, Yuliang Wang, Jhurston Herricks and Younan Xia. J. Mater Chem. **14**, (2004) 695.
18. Nuchnapa Tangboriboon, Kittikhun Pakdeewanishsukho, Alexander Jamieson, Anuvat Sirivat, Sujitra Wongkasemjit. Materials chemistry and physics **98**, (2006) 138
19. Dan Wang, Ranbo Yu, N. Kumada, and N. Kinomura. Chem. Mater. **1999**, 11, 2008.
20. Yanting Li, Xiuguo Sun, Huiwan Li, Shaohui Wang, Yu Wei. Powder technology **194**, (2009) 149.

21. Spectrometric Identification of organic compounds, R.M Silverstein (F.X Webster Shun Akari) et al. © 2005 WILEY 7th edition.
22. Handbook of Spectroscopy, Guinter Gauglitz and Tuan Vo-Dinh. © 2003 WILEY-VCH Verlag GmbH & Co. KGaA, Weinheim.
23. Klug, Alexander, X-Ray Diffraction Procedures, 2nd Edition, Wiley Inter Science, USA.
24. http://serc.carleton.edu/images/research_education/geochemsheets/braggslaw.jpg
25. P. Fraundorf and Shuhan Lin (2004) "Spiral powder overlays", *Microscopy and Microanalysis* **10**:S2, 1356.
26. B.D Cullity, Elements of X-Ray Diffraction, Addison-Wesley Publishing Company, Inc., 1956
27. http://wikipremed.com/image_science_archive_th/020700_th/188100_Tetragonal_68.jpg
28. G. Thomas et. al., Transmission electron Microscopy of Materials, John Wiley, 1979.
29. http://www.micromagazine.com/archive/04/07/images/0407MI88b.jpg
30. Ferrer S., Borrás J., Martín Gil J. and Martín Gil F.J. "Thermal studies on sulphonamide derivative complexes". *Thermochim. Acta*, 1989, 147, 321 330; 1989, 153, 205 220; 1991, 185, 315 333.
31. Gottfried W. Ehrenstein et al., Thermal analysis, 2004, Hanser.
32. Kaufmann, Characterization of Materials, 2003, Wiley Inter Science, USA.
33. Sigma Aldrich (97%), Product ID: 5593-70-4.
34. Sd Fine-Chem. limited (99%), Product ID: 38296.
35. Merck (99%), Product ID: 71-36-3.
36. Changshu Yangyuan chemical China (99%), Product ID: 678-90.
37. Nopphawan PHONTHAMMACHAI, Tossaparn CHAIRASSAMEEWONG, Erdogan GULARI, Alexander M. JAMIESON and Sujitra WONGKASEMJIT. Journal of Metals, Materials and Minerals, **12**, (2002) 23.